# Spatial-temporal Analysis of Land Subsidence in Jizan Province for 2019-2024

Roman Shults<sup>1</sup>, Esubalew Adem<sup>2</sup>

<sup>1</sup> Interdisciplinary Research Center for Aviation and Space Exploration, King Fahd University of Petroleum and Minerals, 34463 Dhahran, Saudi Arabia – roman.shults@kfupm.edu.sa

Keywords: Land Subsidence, Spatial-temporal Model, Prediction, SBAS, InSAR, Displacement.

#### **Abstract**

This study provides a vertical displacement analysis of Jizan Province, Saudi Arabia, using InSAR-derived time-series data processed with the Short Baseline Subset (SBAS) technique. Vertical displacements were examined through a simple trajectory model and a spatiotemporal model based on distributed scatterer observations. The research focused solely on remote sensing displacement measurements from 2019 to 2024. Displacement time series were analyzed for 80 spatially distributed points across areas with varying landslide susceptibility. Since the area was not affected by earthquakes during the study period, the simple trajectory model only indicates a general trend. Additionally, the time series was very noisy, making the standard extended trajectory model highly sensitive to local variations. Unlike the spatial-temporal analysis, forecasting with the extended trajectory model was unstable and unreliable. The spatial-temporal model successfully captured patterns of settlement and uplift. Estimated vertical velocities ranged from  $-13 \pm 2$  mm/year for sediments to  $+9 \pm 2$  mm/year for uplift, observed in regions with medium and high landslide activity. The remaining areas are stable. Temporal trends, obtained without external variables, show that displacements are mostly consistent with slow deformation typical of distributed scatterers in arid terrain. This displacement-only assessment provides fundamental insight into the kinematic behavior and serves as a baseline for future data-fusion models that incorporate environmental or human factors.

#### 1. Introduction

The analysis of vertical movements of Earth's surface remains one of the challenging tasks in geospatial analysis. Jizan in Saudi Arabia is a developing province within the Kingdom (Shults et al., 2024). Therefore, geospatial monitoring of Earth's movements is a high priority for various infrastructure and industrial projects. The province has several continuously operating GNSS stations managed by the General Authority for Survey and Geospatial Information, but these are not sufficient for detailed research. Such detailed monitoring is only possible using remotely sensed data, which can be provided by spacebased InSAR (Moreira et al., 2013; Hooper, 2006; Hooper, 2016). Since the study area lacks artificial corner reflectors (Ferretti et al., 2001), the only feasible InSAR data processing method is the Short Baseline Subset (SBAS). A drawback of this method is a significantly higher level of measurement noise. For data processing, Sentinel-2 mission data from 2019 to 2024 was used. A total of 80 points, evenly scattered across the study area, were analyzed, and a time series was generated for these points. Although InSAR data processing strategies are well-studied, further analysis remains a significant challenge.

Over the past decades, many different methods for analyzing time series have been developed. Just to mention the most popular ones, including extended trajectory models (Bevis and Brown, 2014), Kalman filtering with smoothing (Shults et al., 2017), autoregressive integrated moving average (Time Series Analysis, 2015), seasonal autoregressive integrated moving average (Time Series Analysis, 2015), exponential smoothing state-space (Hyndman et al., 2008), long short-term memory (Kong et al., 2025), gradient-boosted trees (Boldini et al., 2023), and XGBoost (Chen and Guestrin, 2016). These methods offer stable solutions and include various hyperparameters for adjustments. Most are based on machine learning approaches. However, a significant limitation of these methods is that they simulate displacements separately for each point. To address this problem, it is recommended to use a spatial-temporal approach that combines

spatial information from neighboring stations with temporal data. This method allows the integration of additional information, resulting in more accurate and reliable predictions, especially when handling noisy data.

This paper analyzes land subsidence time series in Jizan province using a spatial-temporal approach. It is divided into four sections. The second section explains the mathematical background of spatial-temporal analysis. The third section presents the simulation results and discusses several specific cases; afterward, the simulation outcomes are used to generate prediction maps. The final section offers conclusions.

## 2. Spatial-temporal Model

To understand the structure of the time series to be analyzed, the scheme that presents the observation point distribution is presented in Figure 1. The points are scattered unevenly, which highlights the need for applying a spatial-temporal approach.

To create a spatial-temporal model, we used the algorithms considered in (Wackernagel, 2003; Chilès and Delfiner, 2012). These procedures are general and not standardized. Different authors use their own calculation algorithms, so below we outline our simulation strategy. The proposed spatial-temporal simulation strategy suggests building the prediction for the selected point (reference point) using surrounding points located within a predefined radius R around the reference point. Based on preliminary studies, the radius was set to 30 km. Therefore, each point's displacement will be simulated using 4-10 surrounding points. The simulation starts with data structuring. From the time series, the observation matrix was created.

$$Y = \begin{bmatrix} y_1(t_1) & \cdots & y_N(t_1) \\ \vdots & \ddots & \vdots \\ y_1(t_T) & \cdots & y_N(t_T) \end{bmatrix}, \quad (1)$$

<sup>&</sup>lt;sup>2</sup> Space Science and Geospatial Institute, Addis Ababa, Ethiopia – yibrie@gmail.com

where 
$$y_i(t_j)$$
 = displacements  
 $i = 1, ..., N$  = stations  
 $t_1, ..., t_T$  = observation epochs

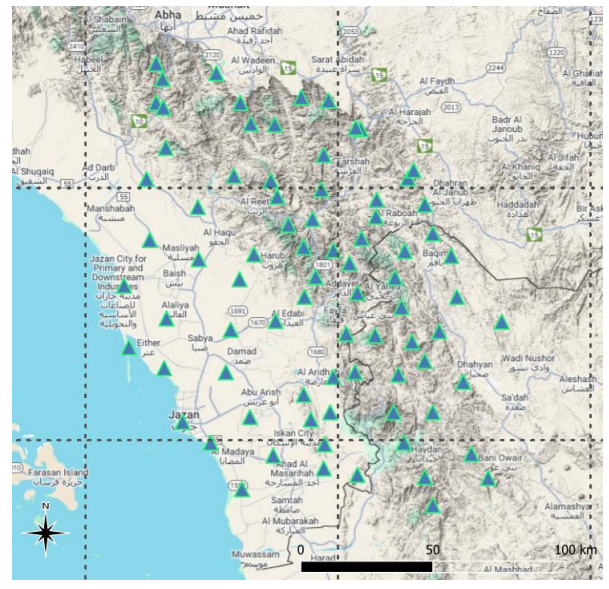


Figure 1. The scheme of observation point distribution.

The general simulation model can be described as a trend/residual Gaussian process/noise. A Gaussian process (GP) is applied to the residuals. Thus, the GP posterior mean at a future time is, by definition, the residual predictive mean.

$$y(t) = m(t, \beta) + r(t) + n(t),$$
 (2)

where  $m(t, \beta)$  = deterministic trend r(t) = latent residual process

n(t) = measurement noise

The initial step of analysis is trend estimation. For the displacements of the chosen reference point, a linear trend model was used:

$$m(t) = \beta_0 + \beta_1(t - t_1),$$
 (3)

where  $\beta_0$ .  $\beta_1$  = trend coefficients

The possible seasonality in displacements was estimated in the covariance below. The trend is removed from all columns. As a result of the detrending, we obtain column-centered residuals (each station's mean removed)  $Y_{res}$  which are used by the stochastic model on the next simulation step. At this step, the spatial-temporal model of a Gaussian process with a Kronecker structure was constructed. A residual field  $r_i(t)$  was simulated as a zero-mean Gaussian with separable covariance:

$$cov[r_i(t), r_i(s)] = K_t(t, s)K_s(i, j) + \sigma_n^2 I\{t = s, i = j\},$$
 (4)

where 
$$K_s(i,j) = \sigma_s^2 exp\left(-\frac{\|x_i - x_j\|^2}{2l_s^2}\right) = \text{spatial kernel}$$

$$K_t(t,s) = \sigma_t^2 exp\left(-\frac{(t-s)^2}{2l_t^2}\right) +$$

$$\sigma_p^2 exp\left(-\frac{2sin^2(\pi|t-s|/P)}{l_p^2}\right) = \text{temporal kernel}$$

$$P = 365.25 \text{ days}$$

 $\sigma_n$  = measurement noise

 $\sigma_s$  = spatial standard deviation (amplitude)

 $\sigma_t$  = smooth (aperiodic) temporal standard deviation

 $\sigma_p$  = periodic (seasonal) temporal standard deviation  $l_s$ ,  $l_t$ ,  $l_p$  = length scales, that show how quickly correlation decays in space/time

Stacking times and points as  $T \times N$ , the full covariance of  $vec(Y_{res})$  will be

$$K = \underbrace{K_t}_{T \times T} \otimes \underbrace{K_s}_{N \times N} + \sigma_n^2 I_{TN}, \qquad (5)$$

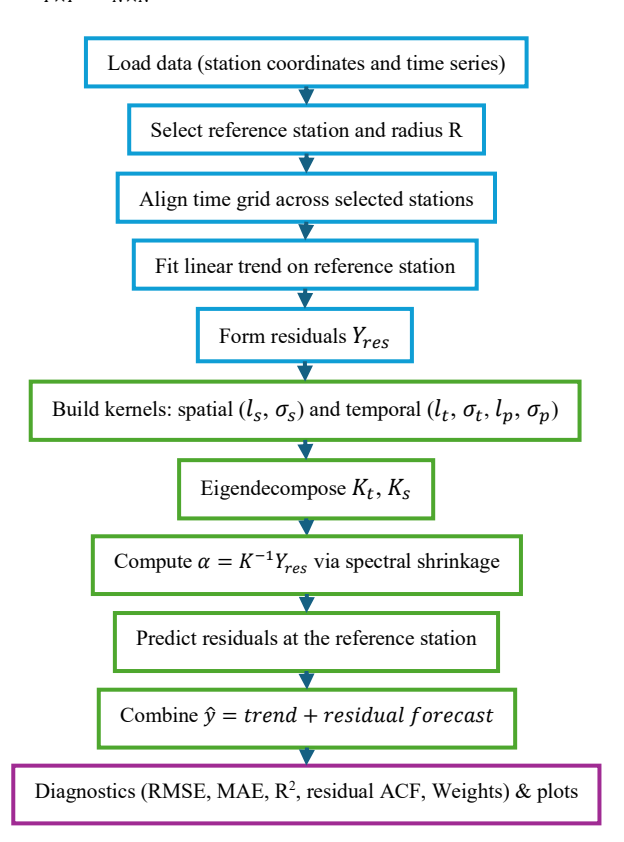


Figure 2. Spatial-temporal simulation flowchart.

The primary goal is to estimate hyperparameters  $\theta = \{\sigma_S, l_S, \sigma_t, l_t, \sigma_p, l_p, \sigma_n\}$  by minimizing the Gaussian process negative log marginal likelihood (NLL) in log-space. Using Kronecker eigendecompositions,  $K_t = U_t diag(d_t)U_t^T, K_S = U_S diag(d_s)U_S^T$  with their eigenvalues for time and space kernel, the NLL and its quadratic term decompose into element-wise operations over eigenpairs, yielding fast and numerically stable optimization. Once we have the estimated hyperparameters, it is possible to predict future displacements using a spatial-temporal Gaussian process model (STGP). Let us suppose we want to predict the displacements of the point  $x_*$  for epochs  $t_1^h, \dots, t_*^h$ , then the STGP gives the residual predictive mean  $\hat{r}_*(t_*^h)$  and variance. The final displacement forecasting model will be

$$\hat{y}_*(t_*^h) = m(t_*^h) + \hat{r}_*(t_*^h), \qquad (6)$$

where h = prediction horizon  $m(t_*^h) = \text{trend prediction}$  $\hat{r}_*(t_*^h) = \text{Gaussian process prediction}$ 

The forecasting process can be shown as a flowchart (Figure 2), which helps make it easier to understand. The described procedure is computationally stable and can be integrated into modern machine learning algorithms.

## 3. Spatial-temporal Analysis

### 3.1 Displacement Simulation

The spatial-temporal analysis can be split into two parts. The first is the model training, and the second is the prediction. To facilitate the model training process, the graphical user interface (GUI) in the MATLAB environment was developed. In this GUI, the user is enabled to upload observation time series and point coordinates. There are two options to tweak the model hyperparameters. The user can assign hyperparameters  $l_s, l_t, \sigma_n$  based on experience or choose between two hyperparameter optimization procedures: k-folds or spatial-LOO. Another option is to apply a periodic time kernel with the following hyperparameters: period (days),  $l_p$ , and  $\alpha_p$  coefficient (0..1). The  $\alpha_p$  value by default was assigned to 0.5. Once the user defines the point of interest and radius, the GUI delivers the list of points that will be used for future spatial-temporal analysis of the point of interest (Figure 3).

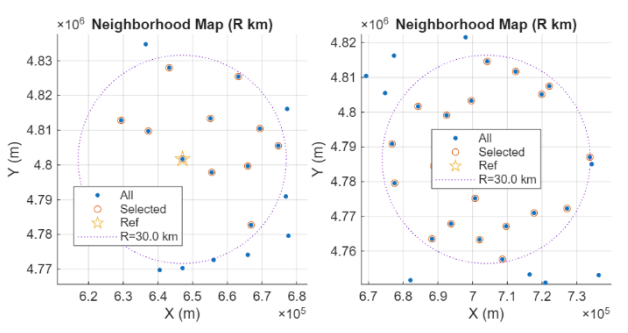


Figure 3. Point selection for spatial-temporal simulation (left – p9, right – p19).

A case study of displacements for points p9 and p19, illustrating settlements and uplift in centimeters, is shown in Figure 4.

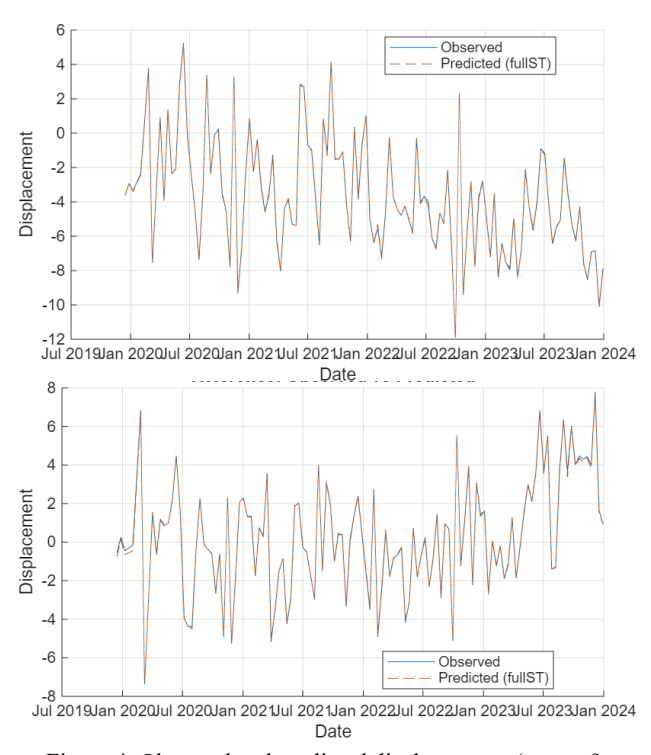


Figure 4. Observed and predicted displacements (top - p9, bottom - p19).

After analyzing the point, the GUI provides simulation diagnostics: root mean square error, mean absolute error,  $R^2$ , and residual autocovariance function (Figure 5). If the trend removal plus space—time GP (including the temporal kernel) is sufficient, the residuals should resemble white noise; that is, the systematic pattern in ACF indicates the model has left some time-dependence in the errors.

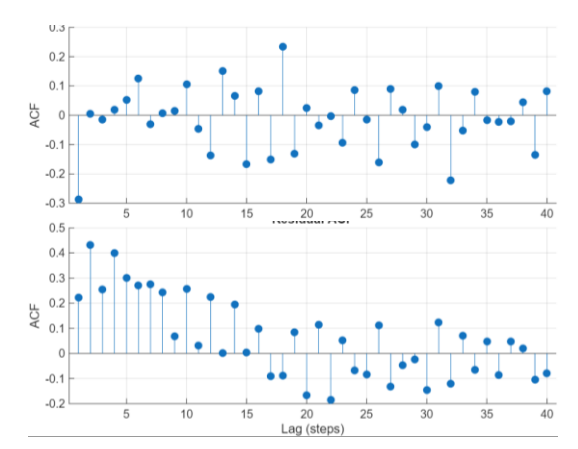


Figure 5. Residual autocovariance functions (top – p9, bottom – p19).

Since the data are very noisy, the residual autocovariance function appears different at various points (Figure 5). In this example, we observe two cases: ACF of p9 – indicating underdamped seasonal mismatch, but all residuals look like white noise, meaning the temporal component is well captured; ACF of p19 shows a slowly decaying tail, indicating long memory is not captured. At other points, different scenarios are also possible, such as a significant positive ACF at small lags or an oscillatory ACF with a clear period. This confirms that the data are too noisy to reliably retrieve the exact signal. Several examples of residual charts after simulation are shown in Figure 6.

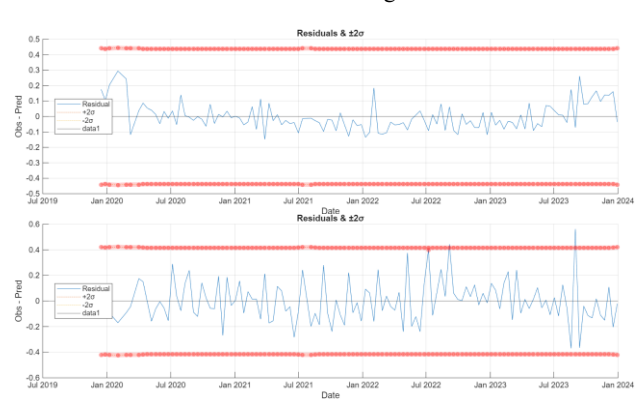


Figure 6. Residual autocovariance functions (top - p72, bottom - p83).

The analysis of simulation diagnostics shows that there is no difference between simulations using a spatial-temporal kernel and a time-periodic kernel. The variation in accuracy metrics was about 0.1-0.3 cm, which is ten times less than the measurement accuracy.

# 3.2 Prediction

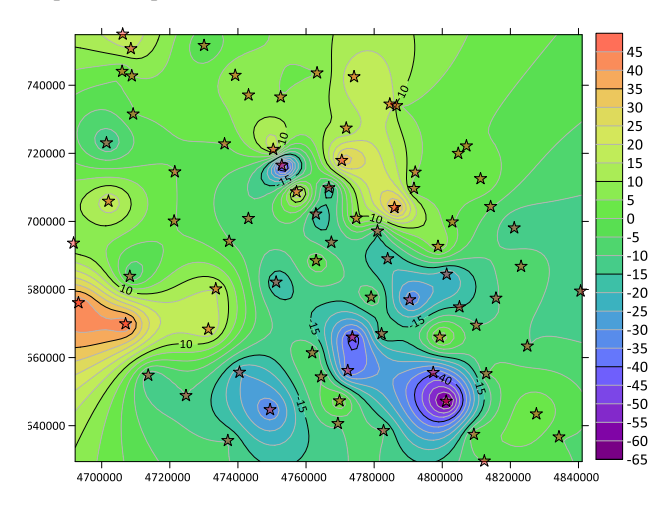
Using the obtained spatial-temporal models for each point, predictions of displacements for all eighty points were generated. The forecasts were made for two periods: 2024-2025 and 2024-

2026. The observed displacements and predictions for 2024-2026 are shown for sampled points in Figure 7.



Figure 7. Displacement predictions for points p9, p19, p50, and p72.

Having predictions for all points, the displacement fields were generated for two epochs. Figure 8 shows displacement fields for a spatial-temporal kernel.



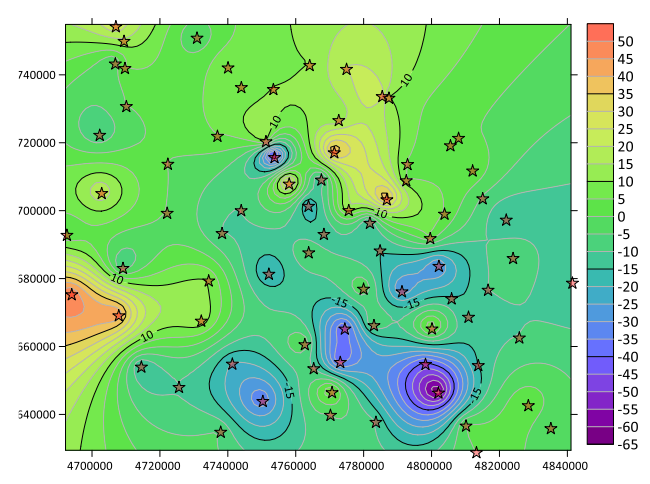


Figure 8. Displacement fields for a spatial-temporal kernel (top – 2024-2025, bottom – 2024-2026).

Figure 9 presents displacement fields for a time-periodic kernel.

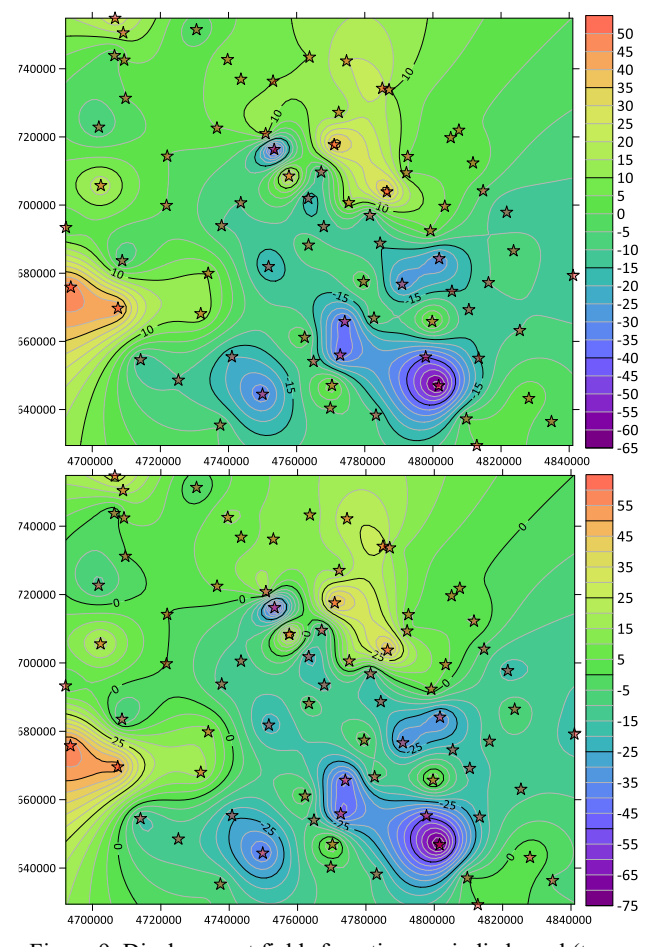


Figure 9. Displacement fields for a time-periodic kernel (top – 2024-2025, bottom – 2024-2026).

A clear understanding of the displacement distribution is reflected in the peaks and depressions chart (Figure 10). This map helps identify regions of surface sediments and uplifts. By comparing this map with a map showing landslide susceptibility regions (Figure 11), one can infer the relationship between the expected displacement values and the level of landslide activity.

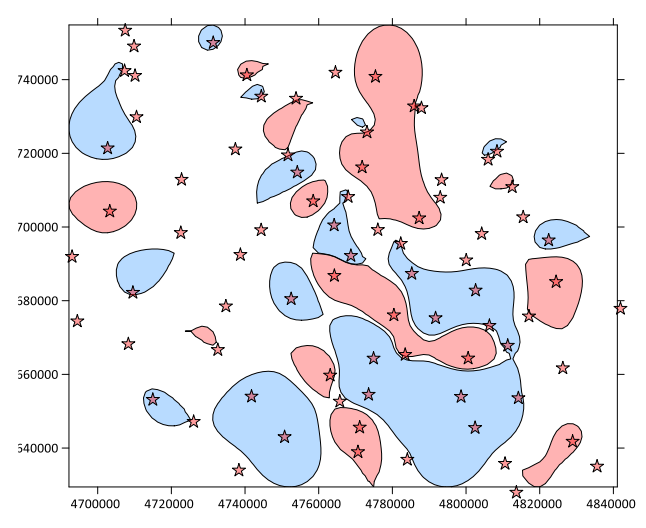


Figure 10. Peaks and depressions map.

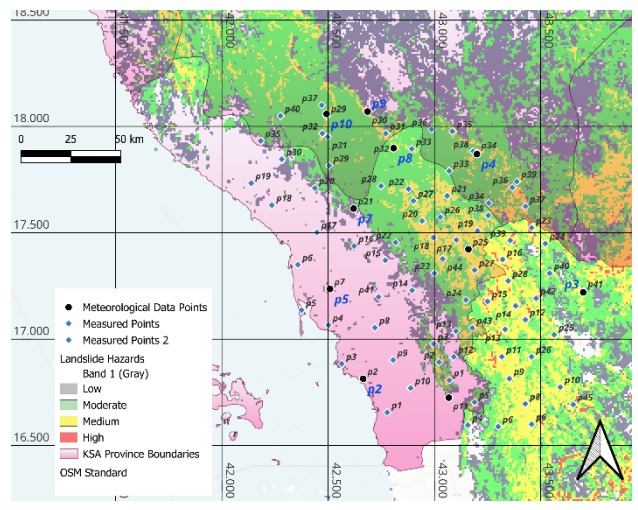


Figure 11. Landslide activity map in Jizan province (geographic coordinates).

The comparison shows mostly zero displacements in areas with low and moderate landslide activity. The significant displacements are mainly found in the southeastern part of the province. This area corresponds to the mountainous region (see Figure 1) and is characterized by medium and high activity. The average displacement velocity for the entire province is -0.6 mm/year. The average sediment velocity is -3.5 mm/year, and the uplift velocity is 3.1 mm/year.

#### Conclusions

This study shows that a displacement-only, spatial–temporal Gaussian-process framework based on SBAS InSAR time series can reliably measure slow vertical movements across Jizan Province from 2019 to 2024, even with high measurement noise. Using 80 distributed points, the spatial–temporal model provided stable forecasts where pointwise trajectory models struggled, and it captured consistent regional patterns of settlement and uplift. Quantitative results include vertical velocities from approximately  $-13\pm2$  mm/yr (subsidence) to  $+9\pm2$  mm/yr (uplift), with the province-wide average near -0.6 mm/yr. Spatially, the largest non-zero movements are found in the mountainous southeast—an area that also has medium—high landslide susceptibility—while zones with low to moderate susceptibility remain mostly stable.

Model diagnostics show that detrending combined with a space-time GP captures most of the temporal structure; residual ACFs are mostly near-white at many locations, although some sites still show low-frequency memory. A periodic time kernel and a fully spatial—temporal kernel provided nearly identical accuracy (differences of about 0.1–0.3 cm), which is much less than the measurement error, emphasizing that spatial coupling—rather than kernel type—drives robustness for this noisy dataset. In contrast, forecasts from the simple trajectory model were unstable and less reliable.

Practically, the results provide: (i) a baseline kinematic map of settlement and uplift magnitudes and how they are spatially arranged; (ii) short- to medium-term forecasts (e.g., 2024–2026) that match the observed dynamics; and (iii) a peaks-and-depressions view that helps identify areas for closer inspection or mitigation. These deliverables are immediately useful for infrastructure monitoring and risk screening in a developing region with limited in-situ instrumentation.

Limitations mainly include reliance on noisy SBAS observations without external drivers, uneven point distribution, and limited independent ground truth. The separable space—time kernel and fixed 30 km neighborhood are practical but may under-model long-memory behavior at some sites.

Future work should therefore focus on (1) integrating data from GNSS, hydrometeorology, groundwater extraction, lithology/land cover, and construction activity; (2) testing non-separable kernels and adaptive neighborhoods; and (3) targeted field validation in the southeastern high-susceptibility belt. Together, these steps would transform the current kinematic baseline into a causal, decision-ready monitoring system for Jizan.

### References

Shults, R., Adem, E., Rahman, M.M., 2024: InSAR-Based Landslide Movement Models: a Case Study of Jizan Province, Saudi Arabia. *IEEE India Geoscience and Remote Sensing Symposium (InGARSS)*, Goa, India, 2024, 1-4, http://doi.10.1109/InGARSS61818.2024.10984378

Moreira, A., Prats-Iraola, P., Younis, M., Krieger, G., Hajnsek, I., Papathanassiou, K., 2013: A Tutorial on Synthetic Aperture Radar. *IEEE Geoscience and Remote Sensing Magazine* 1(1), 6-43. https://doi.org/10.1109/MGRS.2013.2248301

Hooper, A. UNAVCO Training, 2016. Available from: https://www.unavco.org/education/professional-development/short-courses/course-materials/insar/2016-insar-isce-giant-course-materials/Hooper\_Lecture\_PS.pdf. (25 August 2025)

Hooper, A. Persistent scatterer radar interferometry for crustal deformation studies and modeling of volcanic deformation. PhD Dissertation Thesis. Stanford University, May 2006.

Ferretti, A., Prati C., Rocca, F., 2001: Permanent scatterers in SAR interferometry. *IEEE Transactions on Geoscience and Remote Sensing*, 39 (1), 8 – 20. https://doi.org/10.1109/36.898661

Bevis, M., Brown, A., 2014: Trajectory models and reference frames for crustal motion geodesy. *J Geod.*, 88, 283–311. http://doi.org/10.1007/s00190-013-0685-5.

Shults, R., Annenkov, A., 2018: Investigation of the different weight models in Kalman filter: A case study of GNSS monitoring results. *Geodesy and Geodynamics*, 9 (3), 220-228. https://doi.org/10.1016/j.geog.2017.09.003

Time Series Analysis: Forecasting and Control, 5th Edition, by George E. P. Box, Gwilym M. Jenkins, Gregory C. Reinsel and Greta M. Ljung, 2015. Published by John Wiley and Sons Inc., Hoboken, New Jersey, pp. 712.

Hyndman, R., Koehler, A., Ord, K., Snyder, R., 2008: Forecasting with Exponential Smoothing. The State Space Approach. Springer Series in Statistics. Springer Berlin, Heidelberg. https://doi.org/10.1007/978-3-540-71918-2

Kong, X., Chen, Z., Liu, W. et al. 2025: Deep learning for time series forecasting: a survey. *Int. J. Mach. Learn. & Cyber.* 16, 5079–5112. https://doi.org/10.1007/s13042-025-02560-w

Boldini, D., Grisoni, F., Kuhn, D. et al. 2023: Practical guidelines for the use of gradient boosting for molecular property prediction. *J Cheminform.* 15, 73. https://doi.org/10.1186/s13321-023-00743-7

Chen, T., Guestrin, C., 2016: XGBoost: A Scalable Tree Boosting System. KDD '16: Proceedings of the 22nd ACM SIGKDD International Conference on Knowledge Discovery and Data Mining. 785-794 https://doi.org/10.1145/2939672.2939785

Wackernagel, H., 2003: Multivariate Geostatistics. An Introduction with Applications. Springer Berlin, Heidelberg. https://doi.org/10.1007/978-3-662-05294-5

Chilès, J.-P., Delfiner, P., 2012: Geostatistics: Modeling Spatial Uncertainty. John Wiley & Sons, Inc. https://doi.org/10.1002/9781118136188